Ultramicroscopy 145 (2014) 66–73

Contents lists available at ScienceDirect

Ultramicroscopy

journal homepage: www.elsevier.com/locate/ultramic

Atomic resolution imaging and spectroscopy of barium atoms and functional groups on graphene oxide

C.B. Boothroyd [a,*], M.S. Moreno [b], M. Duchamp [a], A. Kovács [a], N. Monge [c], G.M. Morales [c], C.A. Barbero [c], R.E. Dunin-Borkowski [a]

[a] Ernst Ruska-Centre for Microscopy and Spectroscopy with Electrons and Peter Grünberg Institute, Forschungszentrum Jülich, D-52425 Jülich, Germany
[b] Centro Atómico Bariloche, 8400 – San Carlos de Bariloche, Argentina
[c] Department of Chemistry, Universidad Nacional de Río Cuarto, X5804BYA Río Cuarto, Argentina

ARTICLE INFO

Article history:
Received 2 October 2013
Received in revised form
9 February 2014
Accepted 8 March 2014
Available online 19 March 2014

Keywords:
Graphene oxide
Functional groups
Scanning transmission electron microscopy
Transmission electron microscopy
Spectrum imaging
Atomic resolution
Single atom imaging

ABSTRACT

We present an atomic resolution transmission electron microscopy (TEM) and scanning TEM (STEM) study of the local structure and composition of graphene oxide modified with Ba^{2+}. In our experiments, which are carried out at 80 kV, the acquisition of contamination-free high-resolution STEM images is only possible while heating the sample above 400 °C using a highly stable heating holder. Ba atoms are identified spectroscopically in electron energy-loss spectrum images taken at 800 °C and are associated with bright contrast in high-angle annular dark-field STEM images. The spectrum images also show that Ca and O occur together and that Ba is not associated with a significant concentration of O. The electron dose used for spectrum imaging results in beam damage to the specimen, even at elevated temperature. It is also possible to identify Ba atoms in high-resolution TEM images acquired using shorter exposure times at room temperature, thereby allowing the structure of graphene oxide to be studied using complementary TEM and STEM techniques over a wide range of temperatures.

© 2014 Elsevier B.V. All rights reserved.

1. Introduction

Since the discovery of graphene, a huge effort has been made to study graphene oxide (GO), as it is the most promising precursor for producing graphene on a large scale at low cost. In addition, GO and reduced graphene oxide (rGO), in which the C:O ratio is higher than in as-synthesised GO, are versatile and functional materials in themselves for a number of applications that include catalysis, sensing, optical imaging for biological applications and solar cells [1–5].

GO is usually described as a distribution of individual sheets of graphene with oxidised domains, where oxygen-containing functional groups (such as alcohols, epoxy groups, carbonyl groups, hydroxyl groups, carboxylic acids, peroxide, ketones and quinones) are anchored to both sides of the sheet [6,7]. The functionality of GO and rGO results from the extensive presence of these groups, which are suitable for chemical functionalisation [6]. The presence of functional groups necessarily implies that there are defects in the hexagonal graphene lattice, which act as anchoring sites for atoms or groups other than C. At such defect sites, the sp^2 hybridisation of the graphene lattice is not preserved. In general, GO and rGO are considered to be non-stoichiometric materials because the density of oxygenated functional groups and defects cannot be controlled [8–11]. As the high reactivity of GO allows for additional manipulation by controlled chemical functionalisation [12], a broad variety of possibilities that involve non-covalent, covalent or coordinate bonding are available for tailored applications. For example, modification of GO with cations by coordinate bonding has been used to enhance its mechanical properties [13] and to produce gel-like 3D structures [14,15].

Despite its importance, the chemical structures of GO and rGO are still unclear, in part because the compositions and distributions of the functional groups depend on the specific conditions and synthesis methods that are used. The chemical compositions and spatial distributions of the functional groups are of particular importance because they determine most of the properties of both GO and rGO. Most previous work has involved the use of spectroscopic techniques, which provide information that is averaged over a large area of the specimen. For example, it has been reported using infrared and X-ray photoelectron spectroscopies

Abbreviations: TEM, transmission electron microscopy; HRTEM, high-resolution transmission electron microscopy; STEM, scanning transmission electron microscopy; ADF, annular dark-field; HAADF, high-angle annular dark-field; EFTEM, energy-filtered transmission electron microscopy; GIF, Gatan imaging filter; GO, graphene oxide; rGO, reduced graphene oxide; VCA, vertex component analysis

* Corresponding author. Tel.: +49 2461 619279.
E-mail address: ChrisBoothroyd@cantab.net (C.B. Boothroyd).

http://dx.doi.org/10.1016/j.ultramic.2014.03.004
0304-3991/© 2014 Elsevier B.V. All rights reserved.

that thermal reduction of GO occurs in vacuum, changing the C:O ratio [16–18]. More recently, ultrafast optical spectroscopy has been used to determine that GO consists of graphene-like domains surrounded by oxygen-rich areas [8].

High-resolution transmission electron microscopy (TEM) and scanning TEM (STEM) can be used to reveal the presence of both ordered regions and amorphous materials in GO. The amorphous areas are assumed to be highly defective regions in the substrate, to which functional groups are anchored [19,20]. However, the direct identification of individual functional groups has not been possible, as it is not straightforward to distinguish them from amorphous contaminants or to identify individual C and O atoms.

One approach that can be used to identify functional groups in GO and to map their positions is to modify the GO using metal ions, such as Ba^{2+} or Cs^{+}, which interact selectively with specific oxygen-containing groups. Barium ions can form complexes with oxygen-containing groups either on their own [21] or in combination with carboxylates [22] or carbonyl groups [23]. The complexes with carboxylate groups are strong enough to build coordination polymers [24]. Therefore, it is likely that Ba^{2+} ions attach by interaction with the carbonyl, epoxy and carboxylate groups on the surface of GO, but are more strongly attached to the carboxylate groups, making selective staining of these groups possible. The distribution of the heavy atoms, which provide distinct contrast in both high-angle annular dark-field (HAADF) STEM and high-resolution transmission electron microscope (HRTEM) images, rather than the functional groups themselves, can then be imaged. Although Bai et al. [15] modified GO with heavy ions such as Ag^{+} and Pb^{2+}, we believe that the results that we present below provide the first example of the modification of GO using heavy atoms specifically for the purpose of attempting to visualise oxygenated groups in GO. Moreover, the chemical natures of Ba^{2+} and Cs^{+} make it very unlikely they will be reduced to metal (to form nanoparticles), whereas Ag^{+} and Pb^{2+} are reduced more easily.

Here, we show how a combination of complementary TEM techniques can be used to identify Ba atoms on graphene oxide and to determine their positions with atomic spatial resolution. From their locations, it is in principle then possible to infer the positions of the oxygenated functional groups to which they are attached. It is also of interest to examine how the distributions of the functional groups change with increasing temperature, as the more weakly bound functional groups should then be lost, together with any Ba atoms that are attached to them, allowing the functional groups to be identified. For this reason, we used a highly stable single tilt specimen holder based on microelectromechanical systems (MEMS) technology (DENSsolutions, Delft, The Netherlands), which allows specimens to be heated in situ in the TEM to temperatures of up to 1000 °C with no significant loss of spatial resolution and negligible specimen drift. While contamination of the specimen by adsorbed hydrocarbons was always a problem during the examination of GO using STEM imaging and spectroscopy at room temperature, it was discovered during heating experiments that contamination was completely eliminated above a specimen temperature of 400 °C, allowing STEM spectrum images to be acquired over periods of ~15 mins. It is not clear why such high temperatures were required to completely eliminate contamination. Only a small region near the centre of the specimen is heated, so one possibility is that significant hydrocarbons can still migrate from the lower temperature region surrounding the heated area. Without the elimination of contamination by heating the specimen, the experiments that are described below would not have been possible.

2. Experimental details

GO was synthesised from graphite flakes (Sigma-Aldrich) by using an improved method developed by Marcano et al. [25]. Briefly, 9.0 g of $KMnO_4$ was added to a 9:1 mixture of concentrated H_2SO_4/H_3PO_4 (180:20 mL) while stirring. Then, 1.5 g of graphite flakes was added to form a uniform suspension, which was further stirred and heated to 50 °C for 12 h. The reaction mixture was cooled to 5 °C and poured onto ice (200 mL) with 30% H_2O_2 (1.5 mL). The filtrate was centrifuged at 3000 rpm for 1 h and the remaining yellow solid was washed in succession using a 30% HCl solution several times and three portions of water-free ethanol (100 mL). The resulting solid was further washed with Type I water (18 MΩ-cm, ELGA, Purelab Classic) and put into a 10% solution of the trisodium salt of ethylenediaminetetraacetic acid (EDTA) at a pH of ~8 to remove the divalent ions. The mixture was then dialysed against an aqueous solution of HCl (0.05 M) for 24 h and dialysed (Viking C65, diameter 6.5 cm, cut-off 6000–8000 Da) against Type I water for 72 h. The purified solid was added to a solution of $BaCl_2$ (0.01 M, pH ~11), stirred for 24 h and dialysed against Type I water for 72 h, with water changes twice per day to remove residual non-bonded ions.

TEM specimens were prepared by diluting the solution with Type I water and then dropping it onto silicon nitride membrane chips that were designed for a MEMS-based heating specimen holder. The membranes each contained a number of holes, across which the GO sheets could be suspended. All experiments were carried out using an FEI Titan 60–300 "Pico" microscope equipped with a probe C_S corrector, a combined image C_S and C_C corrector and a Gatan imaging filter (GIF). A low accelerating voltage (80 kV) was always used to minimise electron beam induced damage. The C_C corrector allows energy-loss TEM images to be acquired using large (e.g., >50 eV) energy-selecting slit widths with no significant loss of spatial resolution. The acquisition of energy-loss images with a spatial resolution of 0.1 nm at 80 kV using a non-C_C-corrected microscope would require the use of a narrow energy-selecting slit, resulting in a very small signal at the energy losses that are of interest here. The image C_S corrector allows a point resolution of 0.08 nm to be achieved at 80 kV, while the probe C_S corrector allows the same resolution to be achieved for HAADF STEM images.

3. Experimental results

3.1. TEM of graphene oxide

Fig. 1a shows a low magnification bright-field TEM image of a typical region of the GO specimen acquired at 800 °C. The brighter areas, e.g., at the top of the image, correspond to thinner regions that were identified using electron diffraction to consist of either one or a few C layers that were aligned in the same orientation. Darker areas in the image correspond to regions where the carbon layer folded over onto itself during specimen preparation. The detailed examination presented below was carried out on the thinner regions. The image shown in Fig. 1a was acquired slightly underfocus to increase the contrast from the functional groups, which are likely to produce the mottled contrast that varies spatially on a length scale of a few nm. Samples that were imaged at room temperature were consistently found to contaminate, with the source of contamination determined to be the GO itself, as other samples imaged under similar conditions did not exhibit similar problems. A contaminated area, resulting from earlier STEM examination, is visible just to the right of the centre of Fig. 1a. Fig. 1b shows an HRTEM image of the same specimen acquired a few nm underfocus. The image shows a distribution of dark dots that are each presumed to correspond to Ba atoms (see below). However, very little contrast is visible from the functional groups on the GO surface.

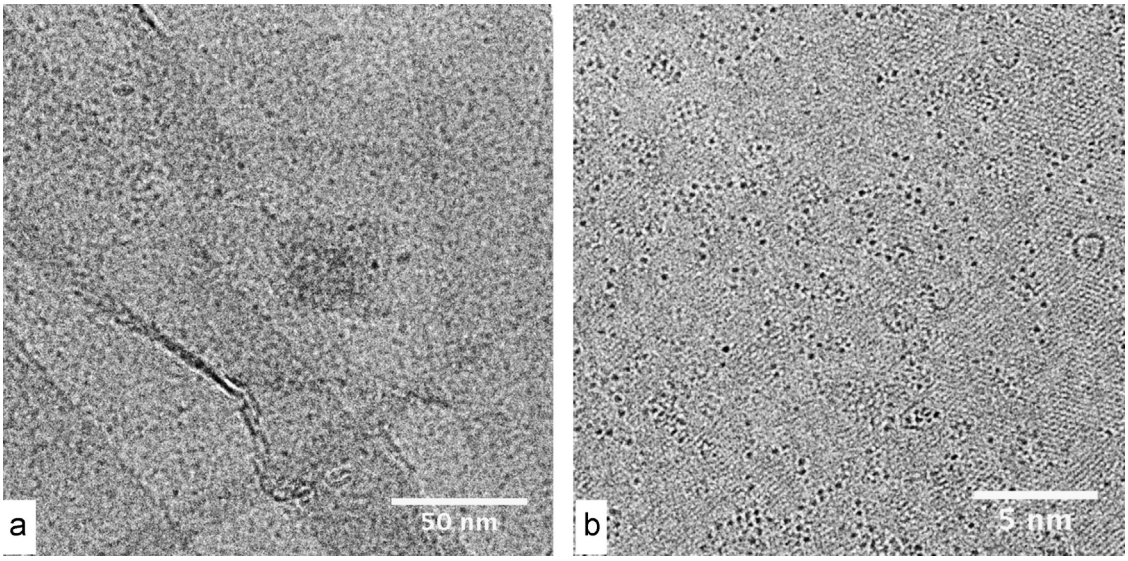

Fig. 1. (a) Low magnification bright-field TEM image of graphene oxide modified with Ba^{2+}, imaged slightly underfocus to enhance the contrast. The lighter regions (e.g., at the top) consist of one or a few layers of graphene oxide. The darker regions (e.g., at the bottom left and right) are areas where the graphene oxide has folded over onto itself. The nanometre-scale contrast is thought to be associated with the presence of the functional groups. The dark area to the right of the centre of the image is a patch of contamination that formed during the acquisition of an earlier STEM image. (b) High-resolution TEM image of a thin area of graphene oxide acquired from a region similar to that shown in (a). Both images were acquired at a specimen temperature of 800 °C and at an accelerating voltage of 80 kV.

Fig. 2 shows an electron energy-loss (EEL) spectrum acquired from a large area (tens of micrometres in diameter) of the same specimen. A strong C K edge is visible at 284 eV. Also present are edges from Ca $L_{2,3}$ at 346 eV, O K at 532 eV and Ba $M_{4,5}$ at 781 eV. The Ba edge is more easily seen in a background-subtracted spectrum, which is overlaid in red onto Fig. 2 above 500 eV. The spectrum confirms that O is present, as expected for GO, with approximately 8 at% O present on average in the thin region analysed. The fine structure of the O K edge shows no distinct features apart from a small shoulder just before the edge, indicating the absence of significant order of the O atoms. This observation is consistent with the random attachment of oxygen atoms to the graphene layer during the oxidation process. It is also consistent with the conventional belief that O-containing functional groups tend to agglomerate to form highly oxidised domains that are surrounded by areas of pristine graphene [26]. The presence of a clear Ba edge in Fig. 2 (corresponding to 0.15 at% Ba) shows that Ba is present on the GO. Just as for the O edge, no fine structure is observed above the Ba white lines, suggesting that the Ba atoms are distributed in an aperiodic manner (although in this case the low signal means that any structure on the Ba edge could be lost in noise). In all of our samples, we also find a small amount (~1.5 at%) of Ca, which may originate from traces of Ca^{2+} in the water that was used during the preparation and/or dialysis process. The Ca^{2+} ions interact with the functional groups as counter-ions or via coordinate bonding. Despite the effort that was made to remove any remaining divalent cations after the oxidation step by reaction with the strong complexing agent EDTA, it appears that it was not possible to remove all of the Ca^{2+}. Future studies will address the possibility of eliminating residual cations.

Attempts were made to image the distribution of each element using energy-filtered TEM (EFTEM) with a GIF. However, the high beam intensities and long exposure times (typically 30 s) that were required, even when using a large (50 eV) energy-selecting slit, resulted in severe damage to the specimen. As a result, the spatial resolutions of the energy-loss images were then limited to ~10 nm or worse and beam damage between exposures meant that the specimen changed during acquisition of each set of three images required to use the standard three-window method for background subtraction. While the use of uniform illumination in EFTEM has advantages for avoiding the effects of contamination, which then occurs mostly at the outer edge of the illuminated area just outside the field of view, for the present specimen it means that the structure must remain drift-free and damage-free over multiple 30 s exposures.

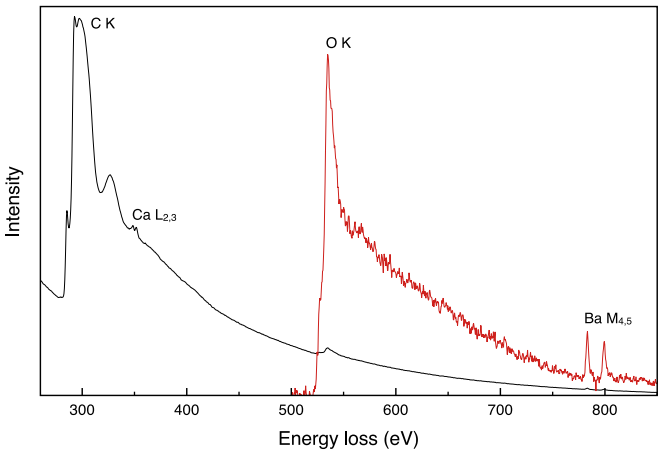

Fig. 2. EEL spectrum recorded from a large area of graphene oxide containing Ba at a specimen temperature of 400 °C, with the C K, Ca $L_{2,3}$, O K and Ba $M_{4,5}$ edges marked. Also shown in red are the O K and Ba $M_{4,5}$ edges after applying background subtraction to the O K edge. Quantification of the areas under the edges indicates that the average composition of this region of the specimen is approximately 90 at% C, 8 at% O, 1.5 at% Ca and 0.15 at% Ba. (For interpretation of the references to colour in this figure caption, the reader is referred to the web version of this paper.)

3.2. Atomic resolution STEM spectrum imaging

Given the difficulties that resulted from loss of spatial resolution due to beam damage during EFTEM imaging in TEM mode, STEM spectrum imaging was used. The technique involves scanning a finely focused electron beam across the area of interest and acquiring an EEL spectrum and an annular dark-field (ADF) image at each pixel. Drift or damage of the specimen results in distortion of the image rather than blurring. In addition, as all energy losses

are acquired simultaneously, motion of the specimen does not affect background subtraction (to first order). Although the use of a focused probe in STEM experiments greatly enhances contamination, it was possible to eliminate this effect in the present experiments by heating the specimen above 400 °C.

STEM spectrum images were acquired at specimen temperatures of 400 and 800 °C in the form of arrays of 200 × 200 spectra (17 × 17 nm) using a dwell time of 0.02 s per spectrum. A relatively large spot size (spot size 6, convergence semi-angle 24 mrad) was used, in order to obtain a strong enough energy-loss signal. As a result, the graphene lattice was not resolved in the recorded spectrum images. The lowest camera length (29.5 mm) was used, together with a 5 mm entrance aperture, to maximise the EEL spectrum collection angle (~40 mrad) and thus the signal. At each point in the spectrum image, an EEL spectrum was acquired with an energy range of 202 to 1025 eV using 2048 channels and a dispersion of ~0.4 eV/channel. Maps showing the Ba, O and Ca edge intensities were then calculated by subtracting a standard AE^{-r} power law background, as shown in Fig. 3. The fitting ranges used for calculating the maps were; Ba $M_{4,5}$, background fit window 580–773 eV, signal integration window 779–805 eV; O K, background fit window 429–526 eV, signal integration window 530–539 eV; Ca $L_{2,3}$, background fit windows 339–344 and 358–364 eV, signal integration window 346–356 eV. Small bright dots are visible in the Ba map (Fig. 3a), while larger regions of bright intensity are visible in the O and Ca maps, which are noisy.

In order to reduce the noise in the elemental maps, the main spectral components were extracted from the EEL spectra using vertex component analysis (VCA) [27–29]. Briefly, the elemental map was divided into three energy ranges, each containing a significant absorption edge: 700–1000 eV for Ba, 450–550 eV for O and 320–520 eV for Ca. The elemental signals were then separated from the background by systematically projecting the 40,000 spectra in the three energy ranges, both with and without pre-Poissonian normalisation of the initial data, onto between 3 and 5 components. Each original spectrum was then expressed as a linear combination of these components. One component from each of the three energy ranges contained the energy-loss edge of interest, as shown in Fig. 4, while the other components contained background signals. The weight of each component (in the present case, the component that contains the signature of the edge of interest) could then be plotted as a function of position in order to obtain a less noisy elemental map.

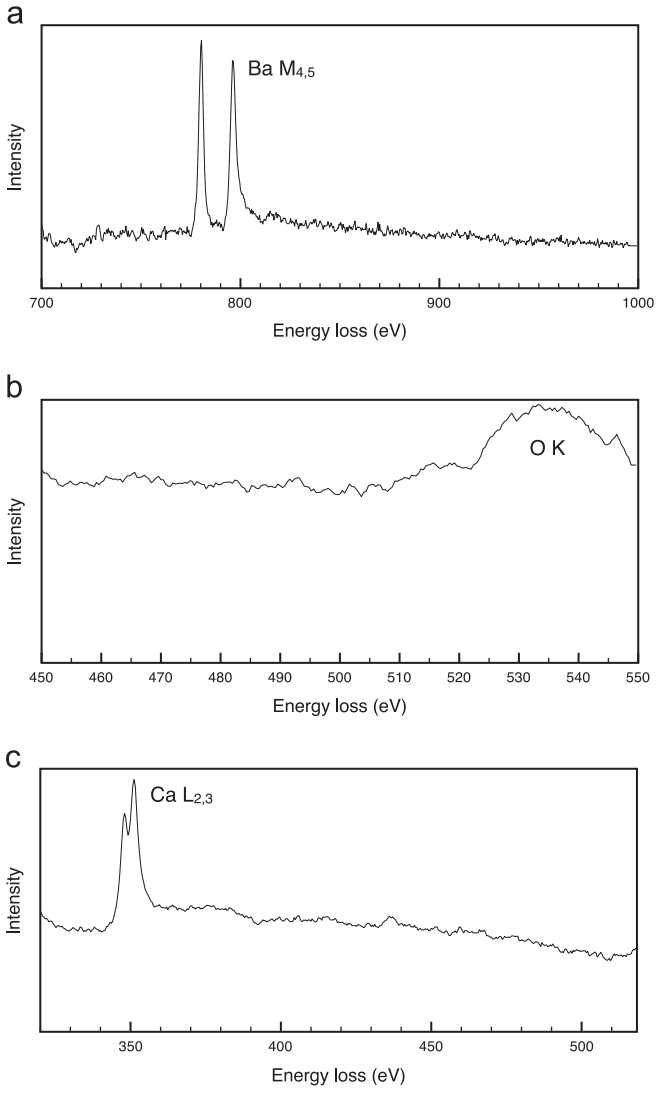

Fig. 4. Spectral components extracted using VCA, corresponding to the following core-loss edges and energy-loss ranges: (a) Ba $M_{4,5}$ and 700–1000 eV, (b) O K and 450–550 eV, (c) Ca $L_{2,3}$ and 320–520 eV. The other spectral components in each energy range contained only background signals.

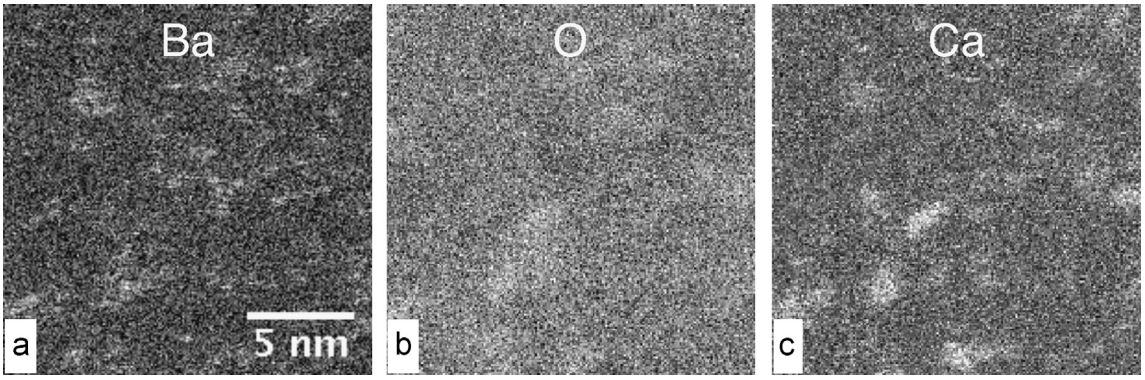

Fig. 3. Spectrum images corresponding to the (a) Ba $M_{4,5}$, (b) O K and (c) Ca $L_{2,3}$ edges, obtained by subtracting a standard AE^{-r} power law background from EEL spectra acquired at each pixel. The following parameters were used: (a) background fit window 580–773 eV, signal integration window 779–805 eV, (b) background fit window 429–526 eV, signal integration window 530–539 eV and (c) background fit windows 339–344 and 358–364 eV (the background was fitted both before and after the Ca $L_{2,3}$ white lines to reduce noise), signal integration window 346–356 eV. The spectra were acquired at a specimen temperature of 800 °C in an array of 200 × 200 spectra using a dwell time of 0.02 s per spectrum. A convergence semi-angle of 24 mrad, a collection semi-angle of ~40 mrad and an energy dispersion of ~0.4 eV/channel were used. The total acquisition time, including the readout time for each spectrum, was approximately 15 mins. The images should be compared with those shown in Fig. 5, which were calculated using VCA. (See text for details).

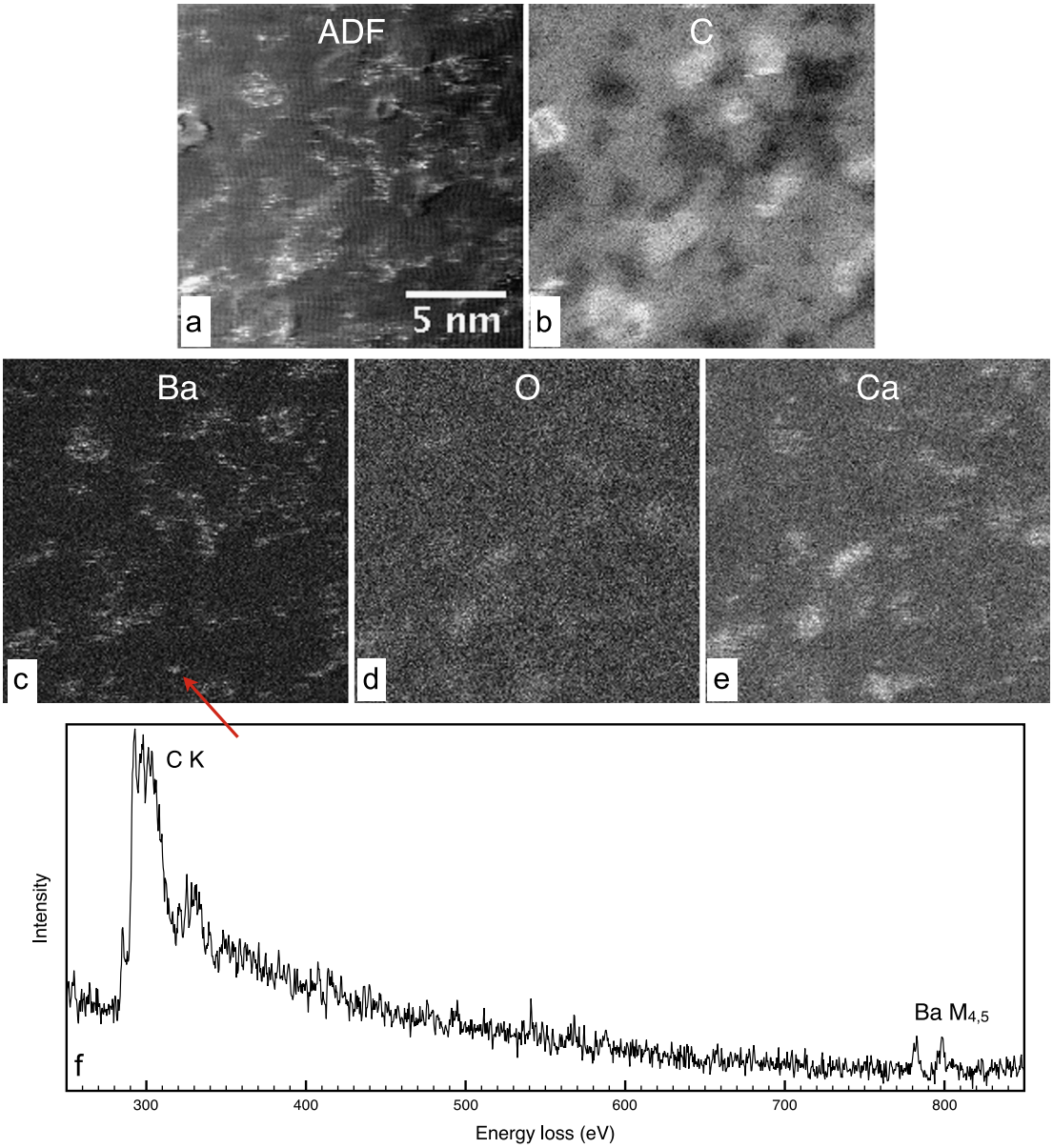

Fig. 5. (a) ADF image and (b–e) spectrum images obtained from the same EEL spectra that were used to generate Fig. 3. The ADF image was acquired at the same time as the EEL spectra using a Gatan ADF detector with an inner radius of ~40 mrad. The spectra were acquired at a specimen temperature of 800 °C in an array of 200 × 200 spectra using a dwell time of 0.02 s per spectrum. The spectrum images correspond to the (b) C K, (c) Ba $M_{4,5}$, (d) O K and (e) Ca $L_{2,3}$ edges. The C K spectrum image was calculated by subtracting a standard power law background, while the Ba, O and Ca spectrum images were calculated using VCA (see text for details). The bright areas in the ADF image correspond to the bright areas in the Ba map, indicating that they correspond to the positions of Ba atoms. The Ca atoms are visible as clusters rather than as individual atoms and exhibit much fainter contrast than Ba in the ADF image shown in (a). (f) EEL spectrum extracted from a 3 × 3 pixel (0.25 × 0.25 nm) part of the spectrum image centred on the Ba atom marked by the arrow. Quantification of the spectrum indicates that the average composition in this region is 5 at% Ba and 95 at% C.

Elemental maps obtained using optimal VCA parameters from the same experimental spectra that were used to generate Fig. 3 are shown in Fig. 5c–e, alongside a C map that was calculated using standard power law background subtraction (Fig. 5b) and an annular dark-field image (Fig. 5a) that was acquired simultaneously with the spectrum image using a Gatan ADF detector surrounding the entrance aperture to the imaging filter (inner radius ~40 mrad). Comparison of the VCA-treated elemental maps (Fig. 5c–e) with the standard background-subtracted maps shown in Fig. 3 highlights the fact that the VCA-treated maps are much less noisy. The features that are present in the VCA-treated maps (Fig. 5) are also present in the standard background-subtracted maps (Fig. 3), suggesting that they are not artefacts introduced by the VCA algorithm.

Examination of the C map (Fig. 5b) shows that there is a range of thicknesses of C present. The areas each appear to be of uniform thickness, suggesting that they correspond to either individual graphene layers or uniform thicknesses of functional groups. Even the darkest (i.e., thinnest) area, near the top right of Fig. 5b, shows some C signal, suggesting that it is not a hole, but comprises a few layers of graphene. The layers have on average approximately 14,000, 18,000, 24,000 and 30,000 counts from darkest to brightest, which is consistent with thicknesses of two to five graphene layers. Some of the thicker areas contain structures that are outlined by bright rings (e.g., slightly above the middle on the left of Fig. 5b; the same bright ring is visible in the ADF image shown in Fig. 5a). This contrast may be associated with graphene layers viewed edge-on, fullerenes or related structures.

The Ba map shown in Fig. 5c contains both isolated bright dots and clusters of bright dots on a uniform background. An EEL spectrum extracted from a small area of size 3×3 pixels (0.25×0.25 nm) around one of the dots is shown in Fig. 5f. The Ba $M_{4,5}$ edge is clearly visible in the spectrum and quantification shows that it contains ~5 at% Ba and ~95 at% C. Allowing for the probe size increasing the irradiated area to approximately 0.3×0.3 nm and assuming that there are three layers of graphene, a value of 9 at% Ba from a single atom would be expected. The area examined may contain additional C from functional groups. In addition, it is unlikely that a Ba atom would remain stationary under the intense electron probe for the full 0.02 s exposure time. Taking all of these factors into account, we believe that the individual bright dots in Fig. 5c correspond to single Ba atoms. The distribution of bright dots in Fig. 5c matches closely with that in the ADF image (Fig. 5a), as would be expected given the high atomic number of Ba. This correlation is important, as it allows the bright dots that are visible in HAADF images to be identified as single Ba atoms.

The signal from O (Fig. 5d) is rather faint, but is concentrated in irregularly shaped areas that are each approximately 2 nm in size. These areas appear to have little correlation with the Ba atom positions, while they do have some correlation with the thinner areas of the C map. However, they do not seem to be distributed around the edges of the thin areas, as is the case for Ba. Fig. 5e shows that the Ca is correlated with the O, suggesting that Ca is bonded to some of the O and may therefore be used as a marker for O. Given that the O signal is faint and that there is more O present than Ca, it is possible that some O is associated with Ba, although at a level that is too low to measure.

The relative distributions of the different species can be seen more clearly when the images are displayed in the form of composite colour maps. Fig. 6 shows the Ba, O and Ca maps together with the C map, which is displayed as a blue background. The Ba and C maps in Fig. 6a confirm that the Ba atoms are concentrated around the edges of the areas where the C is thinner, while very few Ba atoms are seen on the areas where the C is suspected to be ~4 layers thick. The O/C and Ca/C composite maps, which are shown in Fig. 6b and c, respectively, confirm that a significant proportion of the O is associated with Ca and that both elements are present in the thinner areas of the specimen. The Ba/Ca/C composite map in Fig. 6d suggests that Ba and Ca are usually not associated with each other.

3.3. High-angle annular dark-field images

Fig. 7a and b shows two HAADF STEM images, which were collected before and after the spectrum images shown in Figs. 3, 5 and 6. The most prominent contrast in the HAADF images takes the form of bright dots, which are highly likely to correspond to single Ba atoms, based on the correlation between bright dots visible in ADF images (Fig. 5a) and Ba maps (Fig. 5c) presented above. This hypothesis appears to be confirmed by the uniform intensity and shape of the more isolated bright dots, as pairs of Ba

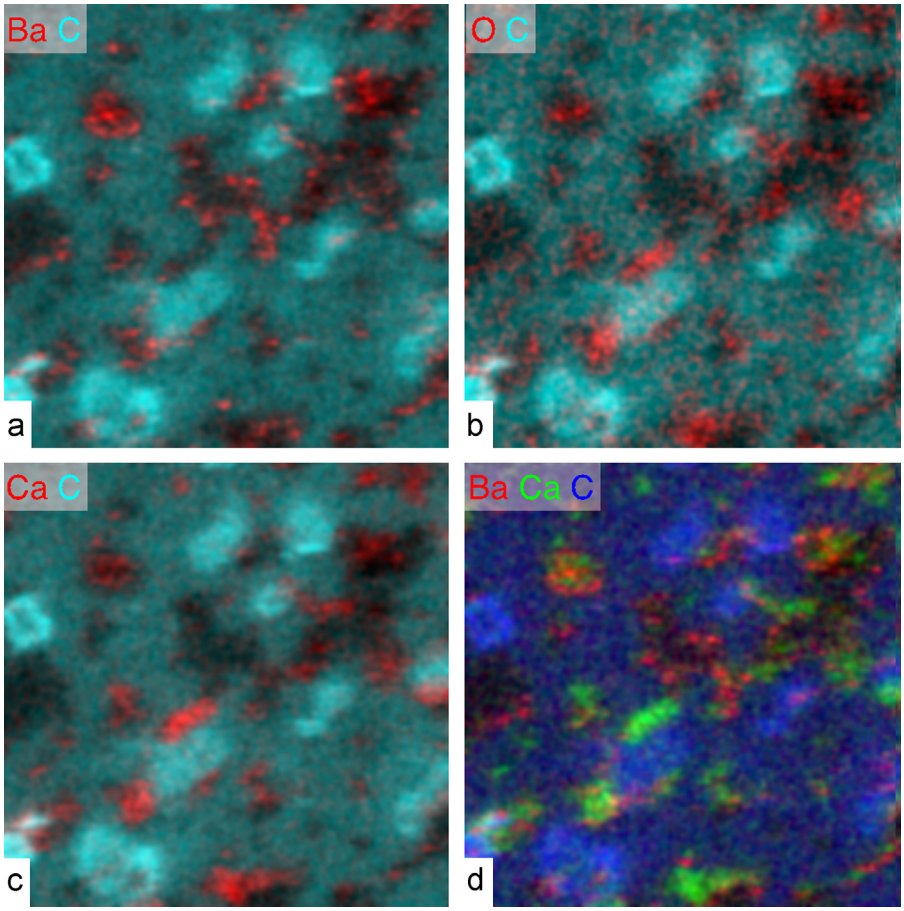

Fig. 6. Composite colour images created from a selection of the spectrum images shown in Fig. 5, which were acquired from graphene oxide with Ba imaged at a temperature of 800 °C. The images show the spatial relationships between the elements, corresponding to the following colours: (a) Ba red and C cyan; (b) O red and C cyan; (c) Ca red and C cyan; (d) Ba red, Ca green and C blue. The spectrum images from Fig. 5 were smoothed using a Gaussian filter of radius 1 pixel and scaled in intensity in order to create the colour images, which show that Ba, O and Ca are present mostly in the areas where the C is thinnest and that Ca and O have very similar distributions. (For interpretation of the references to colour in this figure caption, the reader is referred to the web version of this paper.)

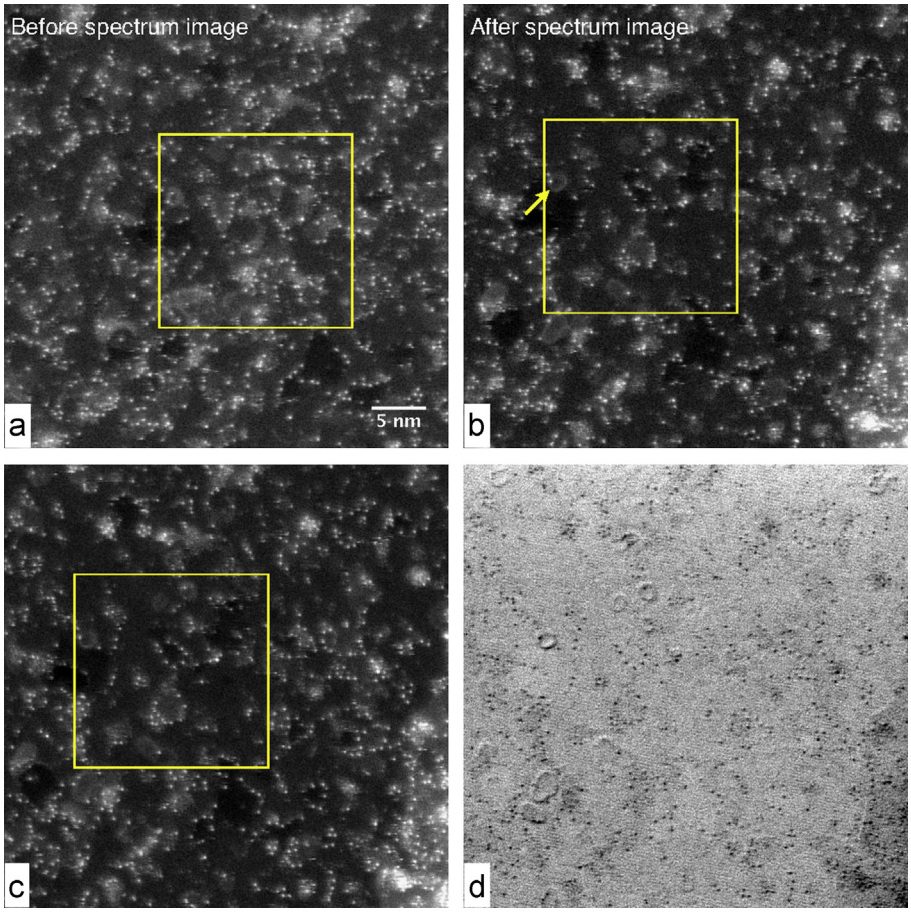

Fig. 7. (a, b) HAADF STEM images acquired at a specimen temperature of 800 °C (a) before and (b) after recording the spectrum image shown in Figs. 5 and 6, whose approximate area is marked by the box. While the area surrounding the box is relatively unchanged after acquiring the spectrum image (except for a small amount of drift and local distortion of the graphene oxide film), the area from which the spectrum image was acquired has changed significantly. (c) and (d) show simultaneously acquired HAADF and bright-field STEM images, respectively, recorded after the spectrum image. The bright dots in the HAADF image correspond to the dark dots in the bright-field STEM image.

atoms would be expected to be resolved and to have elongated shapes.

A greyish background of varying intensity, which is expected to correlate with the thickness of the GO film, is also visible. The ring-like structures that were seen in the C map are also present in the box that marks the area used for the spectrum image (arrowed in Fig. 7b). Although there was a small amount of specimen drift to the left during the 15 min spectrum image acquisition time, the GO that surrounds the spectrum image area is similar before (Fig. 7a) and after (Fig. 7b) acquisition. Although some changes have occurred, such as a thinning of the GO to the bottom left of the spectrum image area, this observation indicates that the GO itself is relatively stable over this time period at the temperature (800 °C) at which the film was held. Closer examination indicates that the positions of the clusters of Ba atoms outside the spectrum image area remain relatively unchanged, while most of the individual Ba atoms within the clusters moved slightly during the time over which the spectrum image was recorded.

Examination of the area of the spectrum image (within the box) in Fig. 7a and b reveals considerable changes to this region of the specimen. The dark hole and the bright ring to the left of the spectrum image area can be recognised in both images, but most of the other features have either changed or are unrecognisable. This difference suggests that great care is required when interpreting both the relative positions of atoms in the spectrum image and their EEL signal, as the beam rearranges their structure. Nevertheless, as the elemental map and ADF image are acquired simultaneously at each pixel, the correlation between the maps still holds and it is possible to state that the bright dots in the ADF image correspond to Ba atoms and that the Ba atoms do not correlate strongly with the O or Ca signals.

Fig. 7d shows a bright-field STEM image that was acquired simultaneously with the HAADF image shown in Fig. 7c. Both images were acquired immediately after recording Fig. 7b. The bright dots in the HAADF image correspond to the dark dots in the bright-field STEM image. As the contrast in a bright-field STEM image is inherently related to the contrast in a TEM high-resolution image (such as that shown in Fig. 1b) by reciprocity, the dark dots in the TEM images are interpreted to be single Ba atoms.

4. Conclusions

The structure and composition of graphene oxide modified with Ba^{2+} have been characterised using several complementary TEM techniques at an accelerating voltage of 80 kV. An elevated specimen temperature was found to reduce electron beam induced contamination, in particular when acquiring electron energy-loss spectrum images. Ba atoms were identified spectroscopically and correlated with contrast recorded at the same time in high-angle annular dark-field STEM images. The measurements also show that Ca and O occur together.

The electron dose that is required to obtain an EFTEM image or an EEL spectrum image with atomic spatial resolution from O or Ba on graphene oxide was found to cause significant beam damage, whether TEM or STEM mode was used. As a result of this damage, in our experiments atomic resolution spectrum imaging of graphene oxide was only possible in STEM mode and then only with the specimen heated above 400 °C in a stable heating holder to prevent contamination.

Despite the presence of beam damage, bright spots in HAADF STEM images of graphene oxide could be identified as single Ba atoms using EELS. Similarly, dark spots in underfocus high-resolution TEM images of the same material were also inferred to be single Ba atoms. As it is possible to acquire high-resolution TEM images with a much lower dose than spectrum images, even in the presence of contamination, they can be used to map the distribution of Ba atoms with little beam damage or contamination over the full range of specimen temperatures. The positions of Ba atoms attached to functional groups on graphene oxide could therefore be mapped with atomic spatial resolution by using a combination of STEM and TEM techniques. The fact that Ca was observed to correlate strongly with O suggests that it could be used as a marker for the positions of O-containing groups.

Acknowledgements

We are grateful for financial support from the European Union Seventh Framework Programme under a contract for an Integrated Infrastructure Initiative, ESTEEM2, as well as from CONICET (Argentina) under the PIP, a postdoctoral fellowship (NM) and an international collaboration between Argentina and Germany funded through a CONICET-DFG grant.

References

[1] Y. Tao, Y. Lin, Z. Huang, J. Ren, X. Qu, Adv. Mater. 25 (2013) 2594–2599.
[2] J. Balapanuru, J.-X. Yang, S. Xiao, Q. Bao, M. Jahan, L. Polavarapu, J. Wei, Q.-H. Xu, K.P. Loh, Chem. Int. 49 (2010) 6549–6553.
[3] Y. Wang, S.J. Zhen, Y. Zhang, Y.F. Li, C.Z. Huang, J. Phys. Chem. C 115 (2011) 12815–12821.
[4] J.-M. Yun, J.-S. Yeo, J. Kim, H.-G. Jeong, D.-Y. Kim, Y.-J. Noh, S.-S. Kim, B.-C. Ku, S.-I. Na, Adv. Mater. 23 (2011) 4923–4928.
[5] R. Romero-Aburto, T.N. Narayanan, Y. Nagaoka, T. Hasumura, T.M. Mitcham, T. Fukuda, P.J. Cox, R.R. Bouchard, T. Maekawa, D.S. Kumar, S.V. Torti, S.A. Mani, P.M. Ajayan, Adv. Mater. 25 (2013) 5632–5637.
[6] D.R. Dreyer, S. Park, C.W. Bielawski, R.S. Ruoff, Chem. Soc. Rev. 39 (2010) 228–240.
[7] D. Yang, A. Velamakanni, G. Bozoklu, S. Park, M. Stoller, R.D. Piner, S. Stankovich, I. Jung, D.A. Field, C.A. Ventrice, R.S. Ruoff, Carbon 47 (2009) 145–152.
[8] Q. Zhang, H. Zheng, Z. Geng, S. Jiang, J. Ge, K. Fan, S. Duan, Y. Chen, X. Wang, Y. Luo, J. Am. Chem. Soc. 135 (2013) 12468–12474.
[9] D. Chen, H. Feng, J. Li, Chem. Rev. 112 (2012) 6027–6053.
[10] S. Mao, H. Pu, J. Chen, RSC Adv. 2 (2012) 2643–2662.
[11] S. Eigler, S. Grimm, M. Enzelberger-Heim, P. Müller, A. Hirsch, Chem. Comm. 49 (2013) 7391–7393.
[12] Q. Tang, Z. Zhou, Z. Chen, Nanoscale 5 (2013) 4541–4583.
[13] S. Park, K-S. Lee, G. Bozoklu, W. Cai, S.T. Nguyen, R.S. Ruoff, ACS Nano 2 (2008) 572–578.
[14] X. Jiang, Y. Ma, J. Li, Q. Fan, W. Huang, J. Phys. Chem. C 114 (2010) 22462–22465.
[15] H. Bai, C. Li, X. Wang, G. Shi, J. Phys. Chem. C 115 (2011) 5545–5551.
[16] M. Acik, G. Lee, C. Mattevi, A. Pirkle, R.M. Wallace, M. Chhowalla, K. Cho, Y. Chabal, J. Phys. Chem. C 115 (2011) 19761–19781.
[17] H.C. Schniepp, J.-L. Li, M.J. McAllister, H. Sai, M. Herrera-Alonso, D.H. Adamson, R.K. Prud'homme, R. Car, D.A. Saville, I.A. Aksay, J, Phys. Chem. B 110 (2006) 8535–8539.
[18] A. Ganguly, S. Sharma, P. Papakonstantinou, J. Hamilton, J. Phys. Chem. C 115 (2011) 17009–17019.
[19] K. Erickson, R. Erni, Z. Lee, N. Alem, W. Gannett, A. Zettl, Adv. Mater. 22 (2010) 4467–4472.
[20] K.A. Mkhoyan, A.W. Contryman, J. Silcox, D.A. Stewart, G. Eda, C. Mattevi, S. Miller, M. Chhowalla, Nano Lett. 9 (2009) 1058–1063.
[21] R. Cacciapaglia, S. Di Stefano, L. Mandolini, J. Am. Chem. Soc. 125 (2003) 2224–2227.
[22] L. Archer, M.J. Hampden-Smith, E. Duesler, Polyhedron 17 (1998) 713–723.
[23] S.C. Thompson, D.J. Cole-Hamilton, D.D. Gilliland, M.L. Hitchman, J.C. Barnes, Adv. Mater. Opt. Electron. 1 (1992) 81–97.
[24] M.L. Foo, S. Horike, S. Kitagawa, Inorg. Chem. 50 (2011) 11853–11855.
[25] D.C. Marcano, D.V. Kosynkin, J.M. Berlin, A. Sinitskii, Z. Sun, A. Slesarev, L.B. Alemany, W. Lu, J.M. Tour., ACS Nano 4 (2010) 4806–4814.
[26] S. Zhou, A. Bongiorno, Sci. Rep. 3 (2013) 2484.
[27] J.M.P. Nascimento, J.M. Bioucas-Dias, IEEE Trans. Geosci. Remote Sens. 43 (2005) 898–910.
[28] N. Dobigeon, N. Brun, Ultramicroscopy 120 (2012) 25–34.
[29] M. Duchamp, M. Lachmann, C.B. Boothroyd, A. Kovács, F.-J. Haug, C. Ballif, R. E. Dunin-Borkowski, Appl. Phys. Lett. 102 (2013) 133902.